



# Mechanical properties and microstructure of heterogeneous commercial pure titanium prepared by rotary swaging and annealing

Jiajun Hu<sup>1</sup>, Dongmei Zhang<sup>1</sup>, Zhaohua Hu<sup>2</sup>, Shuaizhuo Wang<sup>1</sup>, Bo Gao<sup>1</sup>, Yudong Sui<sup>3</sup>, Wenwen Sun<sup>4</sup>, Lirong Xiao<sup>1</sup>, Hao Zhou<sup>1,\*</sup>, and Yonghao Zhao<sup>1,5,\*</sup> 

<sup>1</sup> Nano and Heterogeneous Materials Center, School of Materials Science and Engineering, Nanjing University of Science and Technology, Nanjing 210094, China

<sup>2</sup> Ansteel Beijing Research Institute Co., Ltd, Beijing 102209, China

<sup>3</sup> School of Materials Science and Engineering, Kunming University of Science and Technology, Kunming 650093, China

<sup>4</sup> Department of Materials Science and Engineering, Southeast University, Nanjing 211189, China

<sup>5</sup> School of Materials Science and Engineering, Hohai University, Changzhou 213200, China

**Received:** 16 August 2023

**Accepted:** 19 October 2023

© The Author(s), under exclusive licence to Springer Science+Business Media, LLC, part of Springer Nature, 2023

## ABSTRACT

The industrial applications of commercial pure titanium (CP-Ti) are significantly limited due to the strength-ductility trade-off in metallic materials. The strategy of heterostructured materials has been proposed to design microstructures for desired strength and ductility. To improve the mechanical properties of CP-Ti, a heterostructured rod, consisting of ultrafine fibrous grains and recrystallized grains, was produced by rotary swaging and subsequent annealing. The heterostructured Ti exhibits a high tensile strength of 636 MPa, simultaneously sustaining a high ductility of 11.9%, its tensile toughness is three times that of the swaged sample. The superior mechanical properties are attributed to the significant hetero-deformation induced (HDI) hardening in heterostructured Ti. It is found that the HDI hardening is induced by the interactions between geometrically necessary dislocations (GNDs) and hetero-interfaces.

## Introduction

Commercial pure titanium (CP-Ti) has a broad application in aerospace and biomedical fields owing to its high specific strength, high corrosion resistance, and good biocompatibility [1–3]. However, the low strength of coarse-grained (CG) CP-Ti limits its further applications

[4, 5]. Grain refinement is the most effective method to enhance the strength of metallic materials. In recent decades, severe plastic deformation (SPD) techniques have been developed to produce ultrafine-grained (UFG) or nanocrystalline (NS) materials [6–8]. However, the increase in strength of UFG/NS materials is usually at the cost of ductility due to the limited work hardening

Handling Editor: Naiqin Zhao.

Address correspondence to E-mail: hzhou511@njjust.edu.cn; yhzha@njjust.edu.cn

<https://doi.org/10.1007/s10853-023-09073-3>

Published online: 22 November 2023

capacity [9, 10]. It is necessary to find novel strategies to improve the strength-ductility synergy of CP-Ti.

Recently, the strategy of heterostructured materials (HSMs) has been proposed because of their excellent mechanical properties [11–13]. The superiority in the strength-ductility combination of HSMs has been verified in various metallic materials, i.e., Cu alloys [14, 15], Mg alloys [16, 17], Al alloys [18], low-carbon steels [19], high entropy alloys [20, 21], etc. In terms of Ti plates, heterostructures involving heterogeneous lamellar structure [22], laminated structure [23, 24], and gradient structure [25] have been developed to improve mechanical properties. Especially, the heterogeneous lamellar structured Ti produced by rolling and subsequent annealing has a high strength of ~ 900 MPa and a high ductility of ~ 8%. Such heterostructured Ti plates are usually produced from the severely deformed structure with fine grains and high-density defects, which provides a sufficient driving force for subsequent incomplete recrystallization to obtain the heterogeneous zones, i.e., ultra-fine and coarse grains.

However, it is difficult to produce heterostructured Ti rods through rolling processing. Therefore, the microstructure of Ti rods should be refined by applicable plastic deformation techniques before annealing. Rotary swaging (RS) is a conventional industrial method for deforming bulk metallic rods [26, 27]. The grain size of rods can be significantly refined due to the large equivalent strain and high strain rate [26, 28–30]. For instance, the bulk nanostructured Mg–Gd–Y–Zr alloy rod with an average grain size of 80 nm was produced by four-pass rotary swaging [31]. Consequently, it is promising to fabricate heterostructured Ti rods by rotary swaging and subsequent annealing.

In the present study, heterostructured CP-Ti rods were prepared by RS and annealing. The microstructure and mechanical properties of heterostructured Ti rods were systematically studied. hetero-deformation induced (HDI) stress in the heterostructured samples was investigated through loading – unloading – reloading (LUR) tensile tests. The underlying mechanisms of HDI hardening were explored in depth.

## Material and methods

CP-Ti rod with ASTM Grade 1 was used in this work, the detail chemical composition (wt%) is shown in Table 1. Figure 1 shows an inverse pole figure (IPF) map

of the as-received CP-Ti, which has an average grain size of ~ 15  $\mu\text{m}$ . The pole figure shows that the initial texture intensity of the as-received CP-Ti is weak, and the maximum pole intensity of {0002} plane is perpendicular to the normal direction (ND). A type of four-die rotary swaging machine was employed to process the CP-Ti. The illustration of its operation refers to Ref. [32]. The initial round bar with a diameter of 35 mm was finally swaged to 7.8 mm with an equivalent strain  $\epsilon$  of 3.0. The  $\epsilon$  is calculated by the equation:

$$\epsilon = \ln(A_0/A) \quad (1)$$

where  $A_0$  and  $A$  are the initial and finish cross-sectional areas of the CP-Ti rod, respectively. The RSed rod were annealed for 10 min or 30 min at 450 °C by air colling, which hereafter called RS3.0-10 min and RS3.0-30 min, respectively.

The tensile specimens were cut from the center of RSed rod using wire cutting. The geometric samples' size for tensile testing is shown in Fig. 2. The uniaxial tensile samples were conducted on a Walter + Baiag LFM 20 kN tensile testing machine equipped with an extensometer under a strain rate of  $1 \times 10^{-3} \text{ s}^{-1}$ . The tensile direction is parallel to the swaging direction (SD). The loading–unloading–reloading (LUR) tensile tests were performed using a contacting extensometer at an unloading rate of 50 N/s to 20N and a reloading strain rate of  $2 \times 10^{-4} \text{ s}^{-1}$ . All tensile specimens were polished gradually using a set of sandpapers from 400 to 2000#.

The microstructure was characterized on a transmission electron microscope (TEM TECNAI 20) and a high-resolution field emission Carl Zeiss Auriga scanning electron microscope (SEM). The SEM is equipped with an Oxford Instruments Aztec 2.0 EBSD system (Channel 5 software) for electron backscatter diffraction (EBSD) mapping. All the metallographic sample was cut from the center of swaged rods. The specimens for EBSD characterization were mechanically polished with SiC paper and then electro-polished in a solution containing 90 vol% acetic acid and 10 vol% perchloric acid in a Buehler Electro Met 4 polisher. The voltage and time for electro-polishing is 35 V and 60 s, respectively. The specimens for TEM characterization were polished to a thickness of 60  $\mu\text{m}$  by sandpaper and then punched

**Table 1** Chemical composition (wt%) of the CP-Ti

C	H	O	N	Fe	Ti
0.009	0.005	0.1	0.012	0.021	Bal.

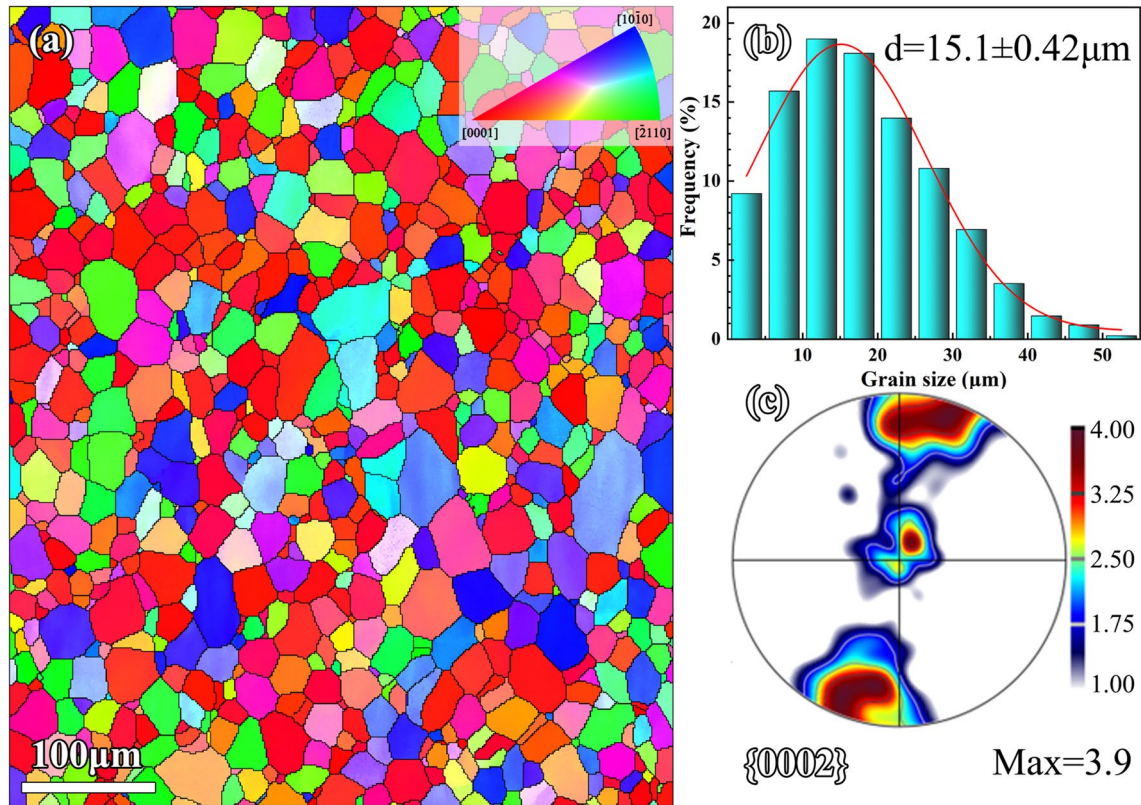


**Figure 1** Microstructure of as-received CP-Ti sample: **a** IPF map; **b** statistical grain size distribution; **c** pole figure of {0002}.

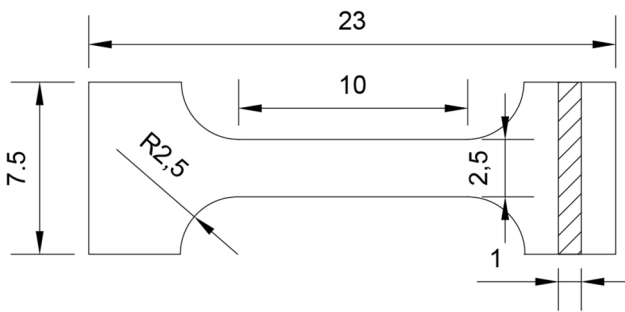


**Figure 2** Geometric dimension of the tensile specimen.

into discs with a diameter of 3 mm. The perforation is carried out by twin-jet electropolishing using a solution of 10 vol% perchloric acid and 90 vol% ethyl alcohol.

## Results and discussion

Figure 3 shows the TEM images of RSed rods with equivalent strains of 1.0 and 3.0. At the equivalent strain of RS is 1.0, a large number of dislocations are

activated in grain interior. High density dislocation cells are discernible along the SD view, marking by the blue arrows in Fig. 3a. Meanwhile, grains are elongated and aligned parallel to the swaging direction, observed along the ND view (Fig. 3b). As marked by the yellow arrows, twins are visible in two directions, which indicate multiple deformation mechanisms are active at the initial stage of RS deformation. With the RS strain increasing ( $\epsilon = 3.0$ ), the grains are significantly refined, forming a fibrous-grained microstructure in width of  $\sim 140$  nm (Fig. 3c and d). Note that, twins are almost absent in this stage. It is revealed that twinning plays the role of coordinated deformation at the early RS stage. However, as the grains gradually refined by the plastic deformation, the activation of twinning becomes more difficult. Such the grain size effect on twinning in pure Ti was reported in the Ref. [26, 33].

Figure 4a-1 and b-1 shows the microstructure in RS3.0-10 min and RS3.0-30 min samples annealed at 450 °C, respectively. After thermomechanical processing, a heterogeneous structure is obtained consisting of equiaxed recrystallized grains and elongation

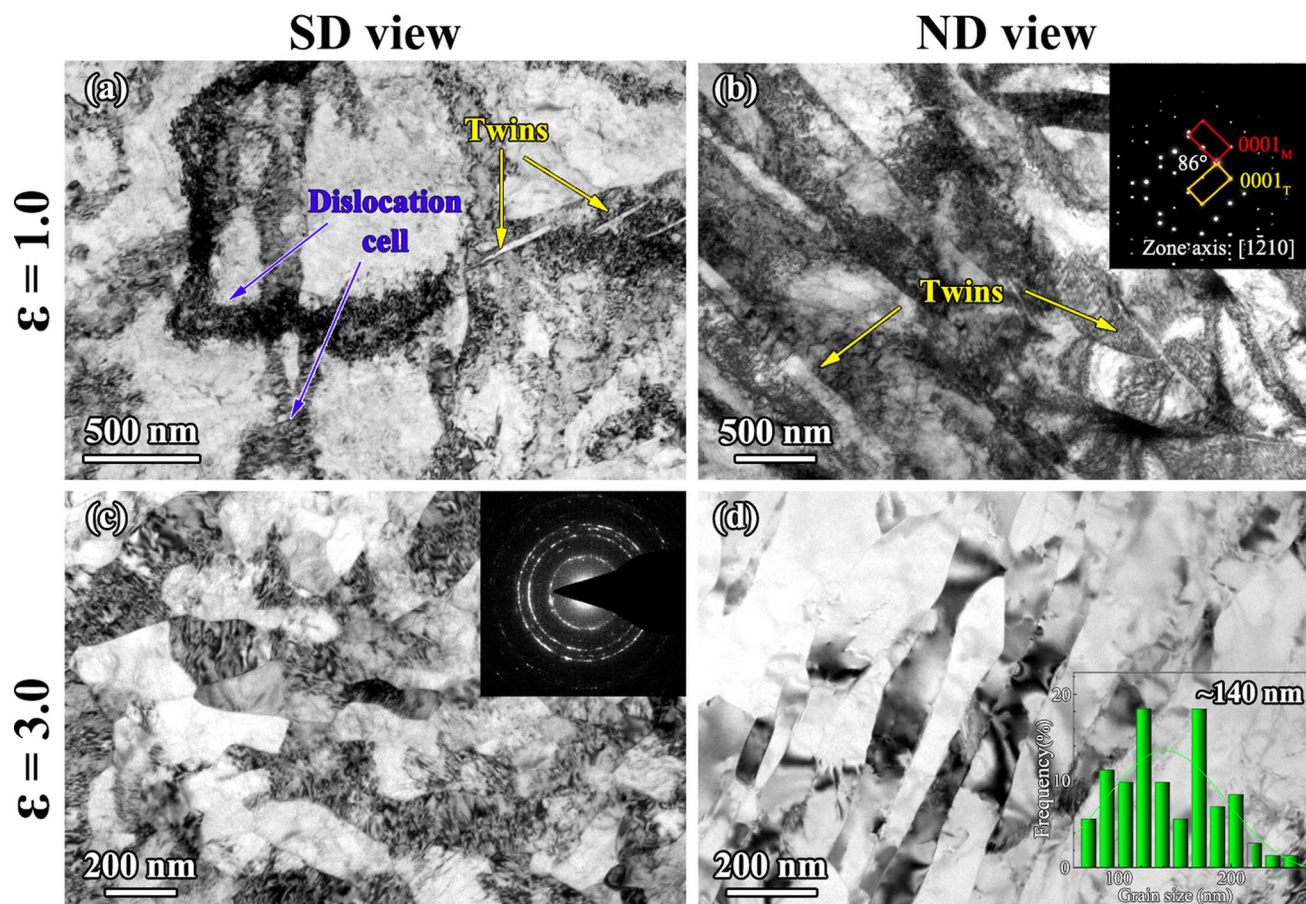


**Figure 3** Bright field TEM micrographs of RS samples: **a** and **b** RS1.0 sample viewed along SD and ND, respectively; **c** and **d** RS3.0 sample viewed along SD and ND, respectively.

fibrous grains. With annealing time increasing, the number and size of equiaxed recrystallized grains increase. In order to quantitatively analyze the size of fibrous grains in IPF maps, the grain size distributions along ND and SD are plotted in Fig. 4a-2 and b-2, denoted by  $d_{ND}$  and  $d_{SD}$ . As annealing time increased from 10 to 30 min, the average length of fibrous grains shows a slightly increasing, whereas the average width is almost unchanged, which is due to the strong texture of annealed RS samples. As demonstrated in Fig. 4a-3 and b-3, a strong  $\langle 10\bar{1}0 \rangle$  texture is formed parallel to the SD in both annealed samples, which indicates that the type of texture is not affected by the increasing annealing time. Grain growth is the migration of grain boundaries, primarily depending on the misorientation between adjacent grains [34, 35]. The smaller misorientation usually leads to easier migration of grain boundaries. In present work, the fibrous-grained microstructure reveals an oriented grain growth, which is achieved by smaller misorientation

between the adjacent grains in SD than those of in ND, during the annealing treatment. Figure 4c and d shows the TEM micrographs in the RS3.0-10 min and RS3.0-30 min samples, respectively. The microstructure of the RS3.0-10 min sample is mainly composed of fibrous ultrafine grains, which contain a little recrystallized grains with grain size less than 1  $\mu\text{m}$ . In contrast, in the RS3.0-30 min sample, the recrystallized grain size reaches 1 ~ 2  $\mu\text{m}$ , forming a typical heterogeneous microstructure morphology.

The engineering stress–strain curves of CP-Ti prepared by RS and subsequent annealing are presented in Fig. 5a. With RS straining up to 3.0, the tensile strength of CP-Ti is reaches from 318 to 813 MPa, while the uniform elongation is decreased from 17.4% to 2.4%. As the annealing time increases, the strength of CP-Ti decreases, while the ductility recovers. Specifically, when the annealing time reaches 30 min, although the strength decreases, its uniform elongation significantly increases, demonstrating excellent

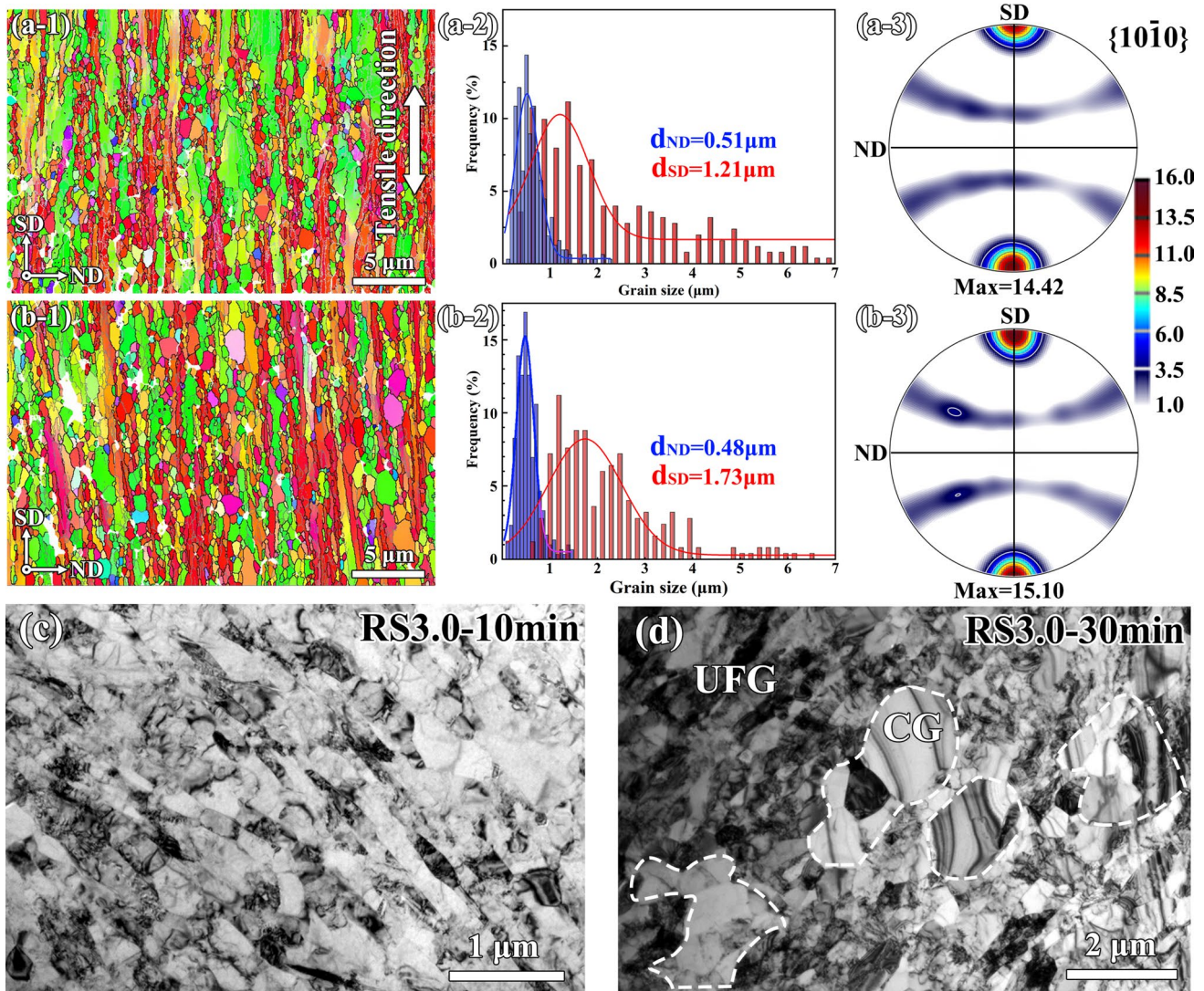


**Figure 4** The evolution of fibrous-grained microstructure annealed at 450 °C: **a-1**, **a-2** and **a-3** IPF map, statistical grain size distribution and pole figure of  $\{10\bar{1}0\}$  of the RS3.0-10 min sample; **b-1**, **b-2** and **b-3** IPF map, statistical grain size distribu-

tion and pole figure of  $\{10\bar{1}0\}$  of the RS3.0-30 min sample; **c**, **d** TEM micrographs of the RS3.0-10 min and RS3.0-30 min samples, respectively.

strength-ductility combination. The work hardening rate ( $\Theta = d\sigma/d\epsilon$ ) versus true strain curves are plotted in Fig. 5b, the RS3.0-30 min sample shows a higher work hardening rate than RS3.0 and RS3.0-10 min samples, which leading to a much higher ductility. We adopted the concept of tensile toughness represented by the product of yield strength (YS)  $\times$  uniform elongation (UE) [36, 37], the value of the RS3.0-30 min sample increased by about three times compared to RSeD sample, as shown in Fig. 5c. This result implied a remarkable enhancement in the combination of strength and ductility of RS3.0-30 min sample. Figure 5d summaries

the YS and the UE of the present samples and those reported in literature for CP-Ti prepared by SPD methods, discovered that the combination of strength and ductility of CP-Ti processed by RS are superior to other SPD processes after annealed. Wang et al. [38] attributed it to the decrease in dislocation density and the strong fiber texture, which leads to the activation of the prismatic and pyramidal  $\langle a \rangle$  slip systems more easily when stretched along the RD. However, in this study, the RS3.0-10 min and RS3.0-30 min samples exhibited similar texture types but different combination of strength and ductility, indicate the existence of

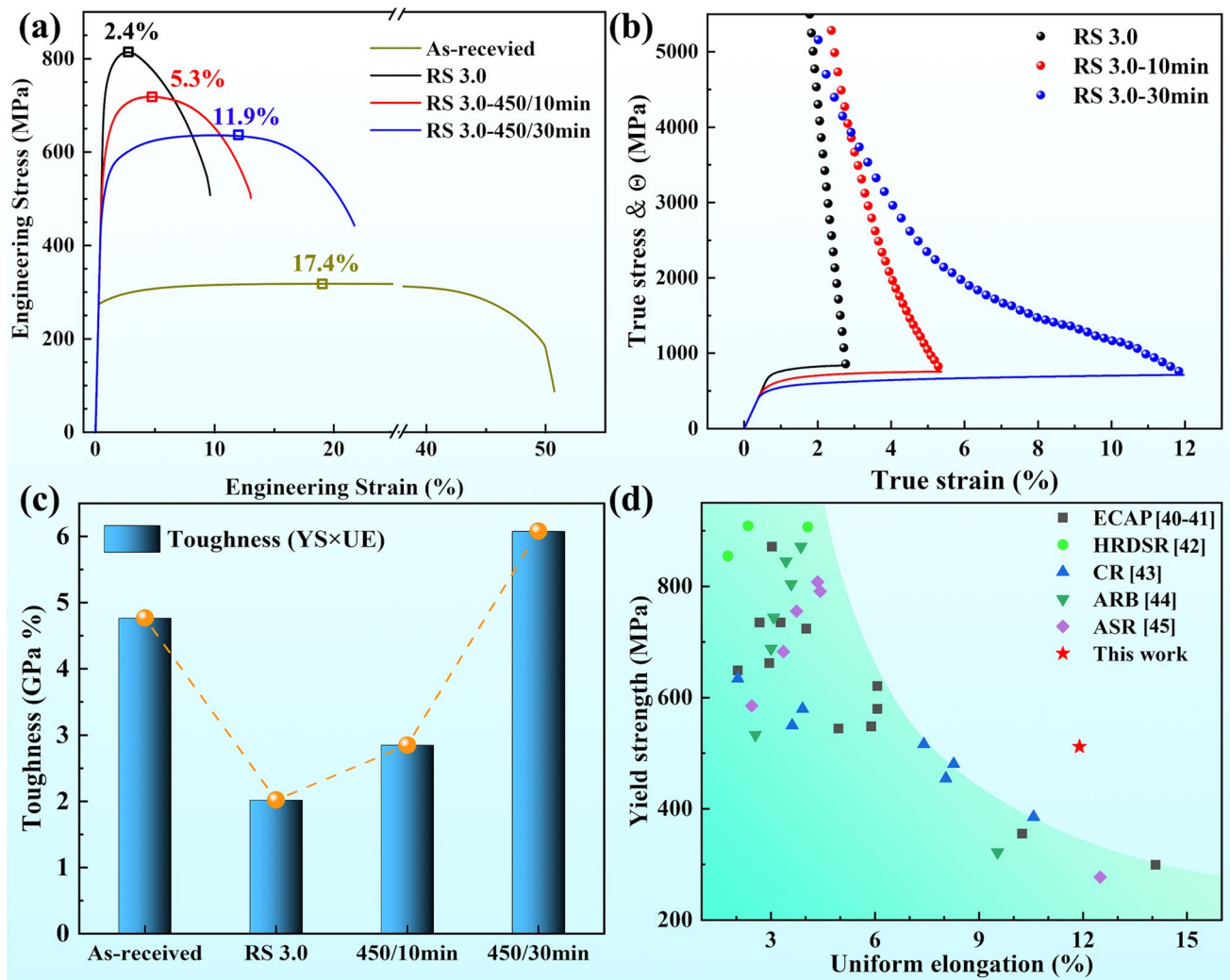


**Figure 5** Mechanical properties of CP-Ti under different treatments. **a** Engineering stress–strain curves; **b** work hardening rate ( $\Theta$ ) and true stress versus true strain curves; **c** toughness of the

annealed sample in comparison with RSeD sample; **d** Comparison of yield strength and uniform elongation of CP-Ti processed with SPD [40–45].

additional strengthening and toughening mechanisms in the RS3.0-30 min sample. Zhu et al. [39] believe that this additional work hardening ability is related to HDI hardening, the strong HDI hardening is superimposed onto the dislocation hardening can improve ductility.

The LUR tensile tests were conducted to investigate the HDI hardening behaviors of RS3.0-10 min and RS3.0-30 min samples, as illustrated in Fig. 6a. The RS3.0-30 min sample exhibits an obvious Bauschinger effect, which shows a larger hysteresis loop during LUR. The HDI stress ( $\sigma_{\text{HDI}}$ ) is calculated by an equation, i.e.,  $\sigma_{\text{HDI}} = (\sigma_u + \sigma_r)/2$ , where  $\sigma_u$  and  $\sigma_r$  represent the unload and reload yielding stress, respectively

[46], as shown in Fig. 6b. The calculation results of  $\sigma_{\text{HDI}}$  are plotted in Fig. 6c-1. Clearly, the HDI stress of RS3.0-10 min sample is higher than RS3.0-30 min sample. Moreover, the loop width (characterized by residual plastic strain,  $\epsilon_{\text{rp}}$ ) of two samples under different strain is measured in Fig. 6c-2. The larger width of loops indicates a stronger HDI hardening [47]. Obviously, the RS3.0-30 min sample has a larger width of loop than the RS3.0-10 min one. For comparing the HDI hardening effect for two samples, the ratio of HDI stress to flow stress in each sample is plotted in Fig. 6d. The ratio of  $\sigma_{\text{HDI}}/\sigma_f$  for RS3.0-10 min sample shows a slow fluctuate with increasing true strain, indicating weak HDI hardening. Moreover, the ratio of  $\sigma_{\text{HDI}}/\sigma_f$

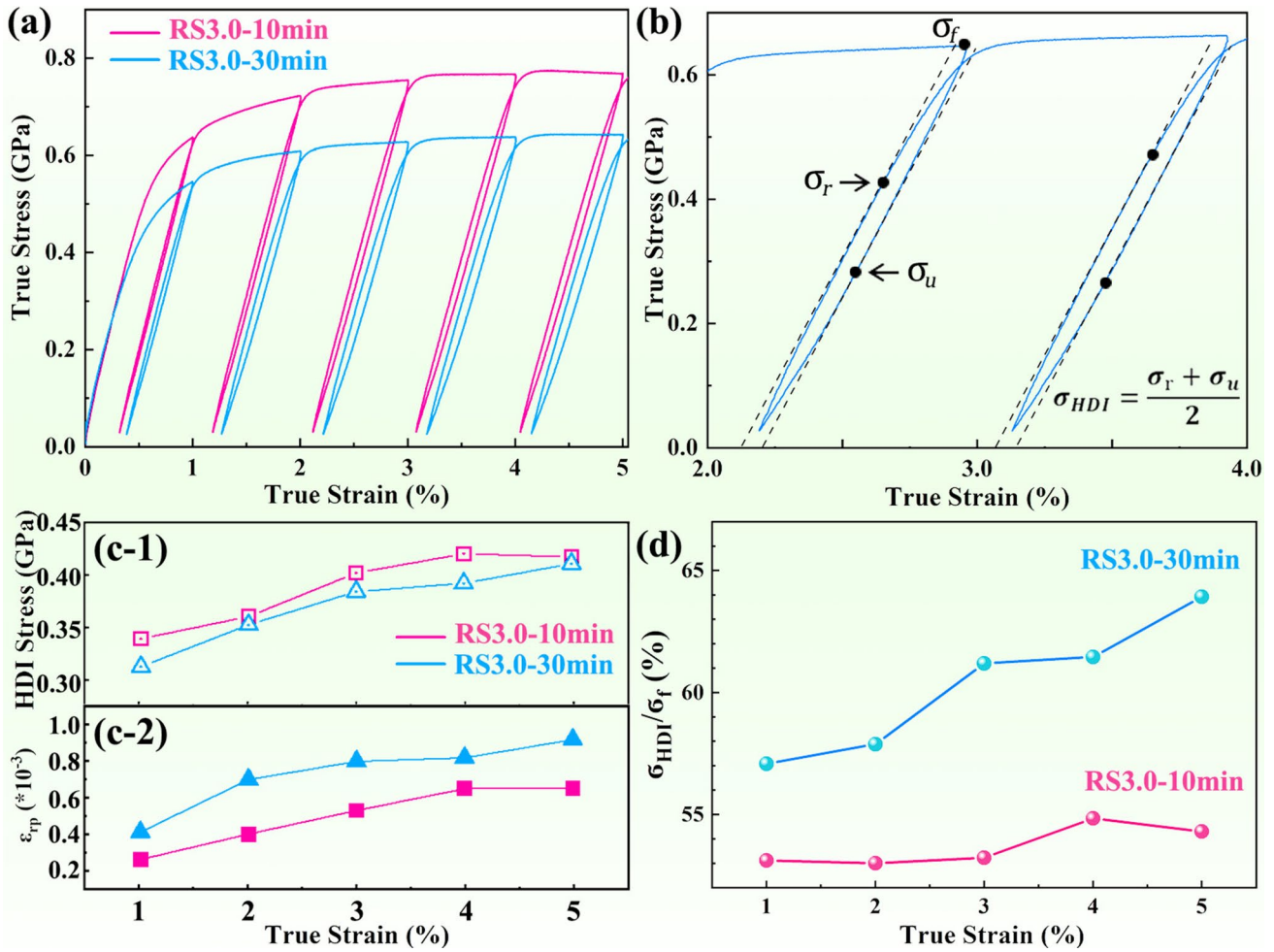


**Figure 6** Analysis of HDI hardening of RS3.0-10 min and RS3.0-30 min samples: **a** load-unload-reload curves; **b** schematic of hysteresis loops for characterizing the Bauschinger effect and the residual plastic strain; **c-1** The calculated results of HDI

stress vs. true strain; **c-2** evolution of the residual plastic strain of hysteresis loops with straining; **d** proportion of HDI stress in flow stress with true strain.

in RS3.0-30 min sample increase with increasing true strain, that more than 60% at true strain larger than 2%, indicating significant HDI hardening effect, which responsible for high work hardening of RS3.0-30 min sample.

The above results show that the HDI hardening effect has a significant impact on the mechanical properties of RS3.0-30 min sample. In order to reveal the origin of this mechanism, the microstructural evolution before and after plastic deformation of RS3.0-30 min sample was investigated by TEM characterization. Figure 7a shows the microstructure before deformation, displaying recrystallized grains have lower density of crystal defects compare with fibrous grains, that's mean, the recrystallized grains

as the soft zone of heterogeneous structure. By contrast, the dislocations pileups are clearly visible at the zone interface in recrystallized grain at an engineering strain of 10%, as marked by the yellow arrows in Fig. 7b. This phenomenon has been reported in lamella heterostructured pure Ti [22]. Since the plastic incompatibility of inter-zone interaction between the soft and hard zones, leading to the generation of strain gradient during plastic deformation. The strain gradient is accommodated by accumulated GNDs which creating the dislocation pileups and generating back stress at the interface of soft zone [11]. In contrast, forward stress is generated on the interface of hard zone, where the back stress and forward stress are the same in magnitude but opposite in directions. The coupling

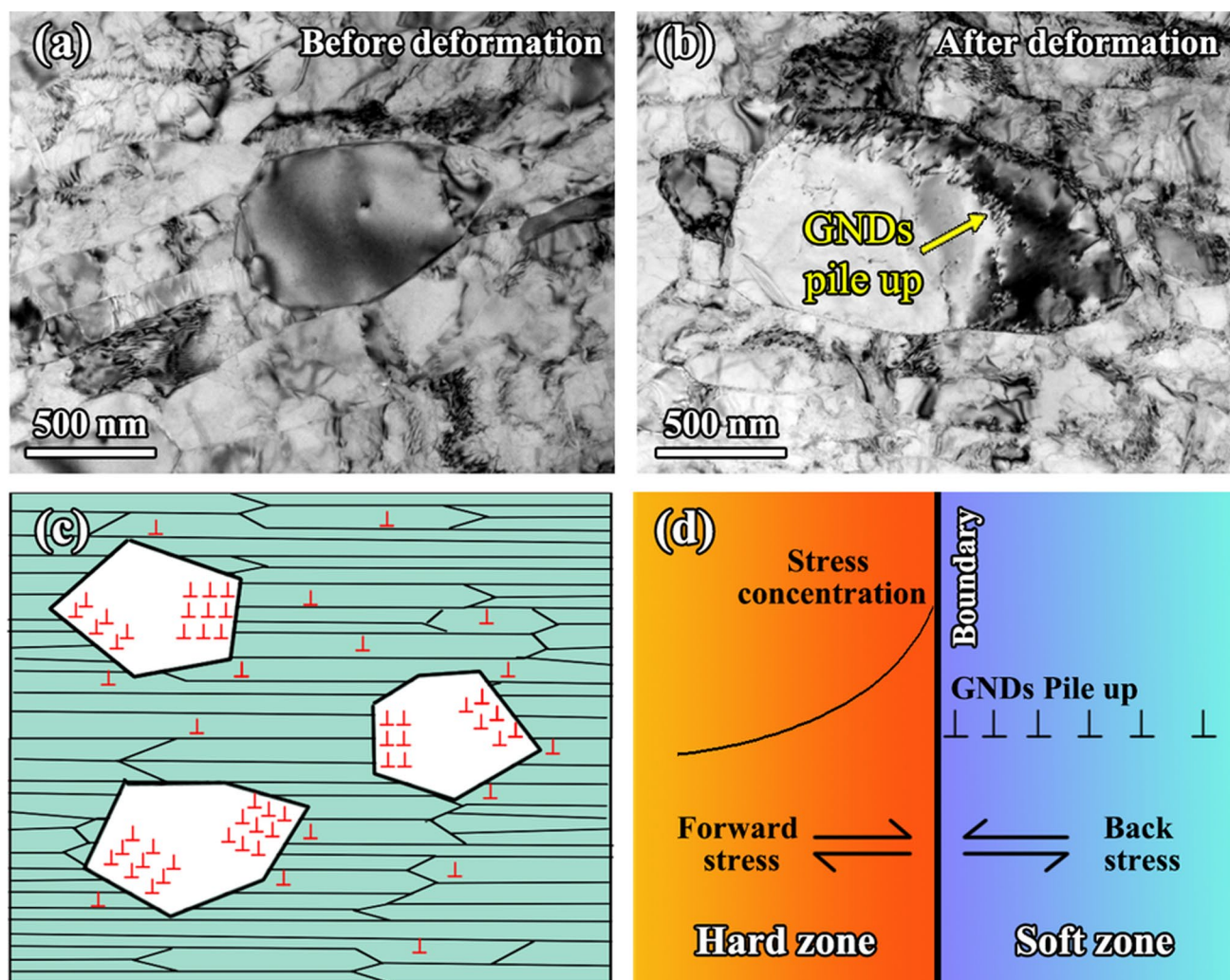


**Figure 7** TEM graphs of RS3.0-30 min sample and schematic of HDI hardening mechanism: **a** before deformation; **b** deformed microstructure at an engineering strain of 10%. **c**, **d** Schematic of

of soft and hard zones produce additional HDI hardening [12], which can be understood with the help of Fig. 7c–d. Since HDI hardening is produced by GNDs pile-up at zone interfaces, the increase in the number of zone interfaces contributes to the formation of HDI hardening [48, 49]. In this study, the heterogeneous CP-Ti, formed through the special deformation method of RS, consists of fiber ultrafine grains and micron recrystallized grains. Compared to lamella heterogeneous materials with the same proportion of soft and hard zones, the CP-Ti has a higher number of heterogeneous interfaces. This increased interface density further enhances the contribution of HDI hardening. Our results expand the understanding of the HDI hardening mechanism in CP-Ti fabricated by RS and

the pile up of GNDs, which produces back stress in the soft zone and forward stress in the hard zone.

annealing techniques. Additionally, we provide a new design method for high interface density heterogeneous structured materials.

## Conclusions

To sum up, the heterostructured CP-Ti rod with enhanced mechanical properties was produced by rotary swaging (RS) and subsequent annealing. The microstructure and mechanical properties of the swaged and heterostructured samples were systematically investigated. The HDI hardening mechanism in heterostructured Ti was analyzed. The key findings of this work are listed as follows:

- (1) The RS processing results in the elongated grains along the swaging direction, forming a fibrous grain structure. The average grain size is significantly refined from  $\sim 15 \mu\text{m}$  to  $\sim 140 \text{nm}$  when the equivalent strain reaches 3.0. As subsequently annealed at  $450 \text{ }^\circ\text{C}$  for 30 min, a heterostructured Ti consisting of equiaxed recrystallized grains and fine lamellar grains was produced.
- (2) The tensile strength of CP-Ti reach to 813 MPa after RS with an equivalent strain of 3.0, while the ductility is significantly reduced to 2.4%. In contrast, the heterostructured Ti shows superior mechanical properties with a high strength of 636 MPa and a high ductility of 11.9%, and its tensile toughness is three times that of the RSed sample. Such a good strength-ductility combination is attributed to the higher work hardening ability of heterostructured Ti.
- (3) The fraction of HDI stress in flow stress is larger than 55% during the entire tensile deformation of heterostructured Ti, thus enhancing the tensile strength. In addition, HDI stress increases with tensile strain, creating an extra HDI hardening, which improves the work hardening ability to maintain ductility. The significant HDI hardening is caused by the GND pile-ups near the zone interfaces during deformation.

## Acknowledgements

This work was supported by the National Key R&D Program of China (grant number 2021YFA1200203), the Key Program of National Natural Science Foundation of China (grant number 51931003), the National Natural Science Foundation of China (grant numbers 51971112, 51225102, 52171118, 52071178, 52201124), Jiangsu Province Leading Edge Technology Basic Research Major Project (BK20222014), the Project Internationalized Construction of Teachers of Jiangsu University (grant number 4023000059), the Fundamental Research Funds for the Central Universities (Grant No. 30919011405), the China Post-doctoral Science Foundation (grant number 2021M701715), the Opening Project of the Key Laboratory of Advanced Manufacturing and Intelligent Technology (Ministry of Education) of Harbin University of Science and Technology (grant

number KFKT202103) and Jiangsu Key Laboratory For Light Metal Alloys (Grant Number LMA202202)

The authors also want to acknowledge the support of the Jiangsu Key Laboratory of Advanced Micro-Nano Materials and Technology. SEM, TEM and EBSD experiments are performed at the Materials Characterization and Research Center of Nanjing University of Science and Technology.

## Author contributions

JH, DZ, and HZ contributed to conceptualization; JH and ZH contributed to methodology; DZ done software; SW and HZ performed validation; JH done formal analysis; JH and DZ done investigation; ZH and YZ helped in resources; JH and DZ helped in writing—original draft preparation; HZ, LX, and BG helped in writing—review and editing; YS and WS done supervision. All authors have read and agreed to the published version of the manuscript.

## Data and code availability

No new data were created or analyzed in this study. Data sharing is not applicable to this article.

## Declarations

**Conflict of interest** On behalf of all authors, the corresponding author states that there is no conflict of interest.

**Ethical approval** The research content of this article does not involve human tissue experiments and is not applicable.

## References

- [1] Peters M, Kumpfert J, Ward CH, Leyens C (2003) Titanium alloys for aerospace applications. *Adv Eng Mater* 5:419–427. <https://doi.org/10.1002/adem.200310095>
- [2] Han P, Xing Y, Yuan G, Zhu X, Wang X (2022) Experimental investigation of the multi-stage micro-deep drawing of pure titanium foils with different grain sizes. *J*

- Mater Sci 57:15094–15108. <https://doi.org/10.1007/s10853-022-07556-3>
- [3] Topolski K, Adamczyk-Cieślak B, Garbacz H (2020) High-strength ultrafine-grained titanium 99.99 manufactured by large strain plastic working. *J Mater Sci* 55:4910–4925. <https://doi.org/10.1007/s10853-019-04291-0>
- [4] Stolyarov VV, Zhu YT, Lowe TC, Valiev RZ (2001) Microstructure and properties of pure Ti processed by ECAP and cold extrusion. *Mater Sci Eng A* 303:82–89. [https://doi.org/10.1016/S0921-5093\(00\)01884-0](https://doi.org/10.1016/S0921-5093(00)01884-0)
- [5] Fattah-alhosseini A, Reza Ansari A, Mazaheri Y, Karimi M, Haghshenas M (2017) An Investigation of mechanical properties in accumulative roll bonded nano-grained pure titanium. *Mater Sci Eng A* 688:218–224. <https://doi.org/10.1016/j.msea.2017.02.013>
- [6] Valiev RZ, Islamgaliev RK, Alexandrov IV (2000) Bulk nanostructured materials from severe plastic deformation. *Prog Mater Sci* 45:103–189
- [7] Zhang M, Liu L, Liang S, Li J (2020) Evolution in microstructures and mechanical properties of pure copper subjected to severe plastic deformation. *Met Mater Int* 26:1585–1595. <https://doi.org/10.1007/s12540-019-00395-z>
- [8] Suryanarayana C (2022) Mechanical alloying: a critical review. *Mater Res Lett* 10:619–647. <https://doi.org/10.1080/21663831.2022.2075243>
- [9] Wang M, Wang Y, He Q, Wei W, Guo F, Su W, Huang C (2022) A strong and ductile pure titanium. *Mater Sci Eng, A* 833:142534. <https://doi.org/10.1016/j.msea.2021.142534>
- [10] Cao Y, Ni S, Liao X, Song M, Zhu Y (2018) Structural evolutions of metallic materials processed by severe plastic deformation. *Mater Sci Eng R Rep* 133:1–59. <https://doi.org/10.1016/j.mser.2018.06.001>
- [11] Wu X, Zhu Y (2017) Heterogeneous materials: a new class of materials with unprecedented mechanical properties. *Mater Res Lett* 5:527–532. <https://doi.org/10.1080/21663831.2017.1343208>
- [12] Zhu Y, Wu X (2023) Heterostructured materials. *Prog Mater Sci* 131:101019. <https://doi.org/10.1016/j.pmatsci.2022.101019>
- [13] Ameyama K, Cazes F, Couque H, Dirras G, Kikuchi S, Li J, Momprou F, Mondal K, Orlov D, Sharma B, Tingaud D, Vajpai SK (2022) Harmonic structure, a promising microstructure design. *Mater Res Lett* 10:440–471. <https://doi.org/10.1080/21663831.2022.2057203>
- [14] Wang YF, Huang CX, He Q, Guo FJ, Wang MS, Song LY, Zhu YT (2019) Heterostructure induced dispersive shear bands in heterostructured Cu. *Scr Mater* 170:76–80. <https://doi.org/10.1016/j.scriptamat.2019.05.036>
- [15] You C, Zeng L, Gao R, Zhang X, Wang H (2022) A dual heterogeneous laminated microstructure design for improving the mechanical properties and electrical conductivity of copper alloys. *Mater Charact* 187:111878. <https://doi.org/10.1016/j.matchar.2022.111878>
- [16] Fu W, Dang P, Guo S, Ren Z, Fang D, Ding X, Sun J (2023) Heterogeneous fibrous structured Mg–Zn–Zr alloy with superior strength-ductility synergy. *J Mater Sci Technol* 134:67–80. <https://doi.org/10.1016/j.jmst.2022.06.021>
- [17] Fu H, Yuan S, Chan KC, Yang X-S (2022) Superior strength-ductility synergy and fatigue resistance of heterogeneous structured AZ41 Mg alloy by laser surface processing. *Mater Sci Eng, A* 858:144151. <https://doi.org/10.1016/j.msea.2022.144151>
- [18] Li D, Wu Y, Geng Z, Zhang J, Chen C, Liu X, Liu Y, Zhou K (2023) High strength Al–Mg–Sc–Zr alloy with heterogeneous grain structure and intragranular precipitation produced by laser powder bed fusion. *J Alloy Compd* 939:168722. <https://doi.org/10.1016/j.jallcom.2023.168722>
- [19] Gao B, Lai Q, Cao Y, Hu R, Xiao L, Pan Z, Liang N, Li Y, Sha G, Liu M, Zhou H, Wu X, Zhu Y (2020) Ultrastrong low-carbon nanosteel produced by heterostructure and interstitial mediated warm rolling. *Sci Adv* 6:eaba8169. <https://doi.org/10.1126/sciadv.aba8169>
- [20] Huang J, Li W, He J, Zhou R, Chou T-H, Yang T, Liu C-T, Zhang W, Liu Y, Huang JC (2022) Dual heterogeneous structure facilitating an excellent strength-ductility combination in an additively manufactured multi-principal-element alloy. *Mater Res Lett* 10:575–584. <https://doi.org/10.1080/21663831.2022.2067790>
- [21] Lu K, Chauhan A, Knöpfle F, Aktas J (2022) Effective and back stresses evolution upon cycling a high-entropy alloy. *Mater Res Lett* 10:369–376. <https://doi.org/10.1080/21663831.2022.2054667>
- [22] Wu X, Yang M, Yuan F, Wu G, Wei Y, Huang X, Zhu Y (2015) Heterogeneous lamella structure unites ultrafine-grain strength with coarse-grain ductility. *Proc Natl Acad Sci USA* 112:14501–14505. <https://doi.org/10.1073/pnas.1517193112>
- [23] Li D, Fan G, Huang X, Juul Jensen D, Miao K, Xu C, Geng L, Zhang Y, Yu T (2021) Enhanced strength in pure Ti via design of alternating coarse- and fine-grain layers. *Acta Mater* 206:116627. <https://doi.org/10.1016/j.actamat.2021.116627>
- [24] Ding H, Cui X, Wang Z, Zhao T, Wang Y, Zhang Y, Chen H, Huang L, Geng L, Chen J (2022) A new strategy for fabrication of unique heterostructured titanium laminates and visually tracking their synchronous evolution of strain partitions versus microstructure. *J Mater Sci Technol* 107:70–81. <https://doi.org/10.1016/j.jmst.2021.08.016>

- [25] Guo Y, Jia B, Zhou Q, Chen W, Ren Y, Zhou Q, Liu R, Arab A, Ran C, Chen P (2023) Enhancement of mechanical properties of commercially pure titanium by shock induced gradient microstructure with martensitic transformation. *Mater Sci Eng, A* 863:144542. <https://doi.org/10.1016/j.msea.2022.144542>
- [26] Meng A, Chen X, Nie J, Gu L, Mao Q, Zhao Y (2021) Microstructure evolution and mechanical properties of commercial pure titanium subjected to rotary swaging. *J Alloy Compd* 859:158222. <https://doi.org/10.1016/j.jallcom.2020.158222>
- [27] Mao Q, Liu Y, Zhao Y (2022) A review on mechanical properties and microstructure of ultrafine grained metals and alloys processed by rotary swaging. *J Alloy Compd* 896:163122. <https://doi.org/10.1016/j.jallcom.2021.163122>
- [28] Mao Q, Zhang Y, Guo Y, Zhao Y (2021) Enhanced electrical conductivity and mechanical properties in thermally stable fine-grained copper wire. *Commun Mater* 2:46. <https://doi.org/10.1038/s43246-021-00150-1>
- [29] Laplanche G, Horst O, Otto F, Eggeler G, George EP (2015) Microstructural evolution of a CoCrFeMnNi high-entropy alloy after swaging and annealing. *J Alloy Compd* 647:548–557. <https://doi.org/10.1016/j.jallcom.2015.05.129>
- [30] Kocich R, Kunčická L, Dohnalík D, Macháčková A, Šofer M (2016) Cold rotary swaging of a tungsten heavy alloy: numerical and experimental investigations. *Int J Refract Metal Hard Mater* 61:264–272. <https://doi.org/10.1016/j.ijrmhm.2016.10.005>
- [31] Wan Y, Tang B, Gao Y, Tang L, Sha G, Zhang B, Liang N, Liu C, Jiang S, Chen Z, Guo X, Zhao Y (2020) Bulk nanocrystalline high-strength magnesium alloys prepared via rotary swaging. *Acta Mater* 200:274–286. <https://doi.org/10.1016/j.actamat.2020.09.024>
- [32] Mao Q, Wang L, Nie J, Zhao Y (2022) Enhancing strength and electrical conductivity of Cu–Cr composite wire by two-stage rotary swaging and aging treatments. *Compos B Eng* 231:109567. <https://doi.org/10.1016/j.compositesb.2021.109567>
- [33] Yu Q, Shan Z-W, Li J, Huang X, Xiao L, Sun J, Ma E (2010) Strong crystal size effect on deformation twinning. *Nature* 463:335–338. <https://doi.org/10.1038/nature08692>
- [34] Humphreys FJ, Hatherly M (2004) *Recrystallisation and related annealing phenomena*, 2nd edn. Elsevier, Oxford
- [35] Miyoshi E, Takaki T, Sakane S, Ohno M, Shibuta Y, Aoki T (2021) Large-scale phase-field study of anisotropic grain growth: effects of misorientation-dependent grain boundary energy and mobility. *Comput Mater Sci* 186:109992. <https://doi.org/10.1016/j.commatsci.2020.109992>
- [36] Li SX, Cui GR (2007) Dependence of strength, elongation, and toughness on grain size in metallic structural materials. *J Appl Phys* 101:083525. <https://doi.org/10.1063/1.2720184>
- [37] Cui GR, Ma ZY, Li SX (2009) The origin of non-uniform microstructure and its effects on the mechanical properties of a friction stir processed Al–Mg alloy. *Acta Mater* 57:5718–5729. <https://doi.org/10.1016/j.actamat.2009.07.065>
- [38] Wang M, Wang Y, Huang A, Gao L, Li Y, Huang C (2018) Promising tensile and fatigue properties of commercially pure titanium processed by rotary swaging and annealing treatment. *Materials* 11:2261. <https://doi.org/10.3390/ma11112261>
- [39] Zhu Y, Ameyama K, Anderson PM, Beyerlein IJ, Gao H, Kim HS, Lavernia E, Mathaudhu S, Mughrabi H, Ritchie RO, Tsuji N, Zhang X, Wu X (2021) Heterostructured materials: superior properties from hetero-zone interaction. *Mater Res Lett* 9:1–31. <https://doi.org/10.1080/21663831.2020.1796836>
- [40] Stolyarov VV, Zeipper L, Mingler B, Zehetbauer M (2008) Influence of post-deformation on CP-Ti processed by equal channel angular pressing. *Mater Sci Eng, A* 476:98–105. <https://doi.org/10.1016/j.msea.2007.04.069>
- [41] Mendes A, Kliauga AM, Ferrante M, Sordi VL (2014) How severe plastic deformation at cryogenic temperature affects strength, fatigue, and impact behaviour of grade 2 titanium. *IOP Conf Ser Mater Sci Eng*. 63:012161. <https://doi.org/10.1088/1757-899X/63/1/012161>
- [42] Kim WJ, Yoo SJ, Lee JB (2010) Microstructure and mechanical properties of pure Ti processed by high-ratio differential speed rolling at room temperature. *Scr Mater* 62:451–454. <https://doi.org/10.1016/j.scriptamat.2009.12.008>
- [43] Zherebtsov SV, Dyakonov GS, Salem AA, Sokolenko VI, Salishchev GA, Semiatin SL (2013) Formation of nanostructures in commercial-purity titanium via cryorolling. *Acta Mater* 61:1167–1178. <https://doi.org/10.1016/j.actamat.2012.10.026>
- [44] Milner JL, Abu-Farha F, Bunget C, Kurfess T, Hammond VH (2013) Grain refinement and mechanical properties of CP-Ti processed by warm accumulative roll bonding. *Mater Sci Eng, A* 561:109–117. <https://doi.org/10.1016/j.msea.2012.10.081>
- [45] Li Z, Fu L, Fu B, Shan A (2012) Effects of annealing on microstructure and mechanical properties of nano-grained titanium produced by combination of asymmetric and symmetric rolling. *Mater Sci Eng, A* 558:309–318. <https://doi.org/10.1016/j.msea.2012.08.005>

- [46] Yang M, Pan Y, Yuan F, Zhu Y, Wu X (2016) Back stress strengthening and strain hardening in gradient structure. *Mater Res Lett* 4:145–151. <https://doi.org/10.1080/21663831.2016.1153004>
- [47] Yang M, Yan D, Yuan F, Jiang P, Ma E, Wu X (2018) Dynamically reinforced heterogeneous grain structure prolongs ductility in a medium-entropy alloy with gigapascal yield strength. *Proc Natl Acad Sci USA* 115:7224–7229. <https://doi.org/10.1073/pnas.1807817115>
- [48] Li N, Cao Y, Liu B, Liu Y (2022) Strengthening mechanism of Ti-W composites with heterogeneous microstructures. *Mater Res Lett* 10:352–359. <https://doi.org/10.1080/21663831.2022.2049907>
- [49] Cui D, Zhang Y, He F, Ma J, Zhang K, Yang Z, Li J, Wang Z, Kai J, Wang J, Jun F (2021) Heterogeneous microstructure of the bonding zone and its dependence on preheating in hybrid manufactured Ti–6Al–4V. *Mater Res Lett* 9:422–428. <https://doi.org/10.1080/21663831.2021.1958947>

**Publisher's Note** Springer Nature remains neutral with regard to jurisdictional claims in published maps and institutional affiliations.

Springer Nature or its licensor (e.g. a society or other partner) holds exclusive rights to this article under a publishing agreement with the author(s) or other rightsholder(s); author self-archiving of the accepted manuscript version of this article is solely governed by the terms of such publishing agreement and applicable law.